EZ-Root-VIS: A Software Pipeline for the Rapid Analysis and Visual Reconstruction of Averaged Root System Architecture

Zaigham Shahzad[1], Fabian Kellermeier[1], Emily M. Armstrong[1], Simon Rogers[2], Guillaume Lobet[3,4], Anna Amtmann[1*] and Adrian Hills[1*]

[1] Institute of Molecular, Cell and Systems Biology, University of Glasgow, G12 8QQ, UK
[2] School of Computing Science, University of Glasgow, G12 8QQ, UK
[3] Agrosphäre (IBG-3), Forschungszentrum Jülich GmbH, Jülich, 52428, Germany
[4] Earth and Life Institute, Université catholique de Louvain, Louvain-la-Neuve, 1348, Belgium

*Corresponding Authors:
Anna Amtmann anna.amtmann@glasgow.ac.uk, Adrian Hills Adrian.hills@glasgow.ac.uk

Short title: Reconstructing root architecture.

One-sentence summary:
EZ-Root-VIS is a new, free, software package that enables the rapid quantification and visual reconstruction of averaged root system architectures for investigating environment-genotype interactions.

Author contributions:
The EZ-Root-VIS pipeline was conceived by F.K. and A.A., and developed by A.H with inputs from S.R. and G.L.. Root growth rate assays were carried out by F.K.. GWAS and genotype-environment interaction studies were designed and performed by Z.S.. E.M.A. helped with the development of the software pipeline and tested the most recent versions using experimental data. AA managed the project. Z.S., A.A., and A.H., wrote the paper.

Funding sources:
The work was funded by the BBSRC (BB/N018508/1) and by the Gatsby Charitable Trust (Sainsbury studentship to FK).

ABSTRACT

If we want to understand how the environment has shaped the appearance and behavior of living creatures we need to compare groups of individuals that differ in genetic make-up and environment experience. For complex phenotypic features, such as body posture or facial expression in humans, comparison is not straightforward because some of the contributing factors cannot easily be quantified or averaged across individuals. Therefore computational methods are used to reconstruct representative prototypes using a range of algorithms for filling in missing information and calculating means. The same problem applies to the root system architecture (RSA) of plants. Several computer programs are available for extracting numerical data from root images but they usually do not offer customized data analysis or visual reconstruction of RSA. We have developed Root-VIS, a free software tool, which facilitates the determination of means and variance of many different RSA features across user-selected sets of root images. Furthermore, Root-VIS offers several options to generate visual reconstructions of root systems from the averaged data to enable screening and modelling. We have confirmed the suitability of Root-VIS, combined with a new version of EZ-Rhizo, for the rapid characterization of genotype-environment interactions and gene discovery through genome-wide association studies in Arabidopsis.

INTRODUCTION

Roots play a critical role in soil water and nutrient uptake and thus in plant productivity. Root system architecture (RSA) is determined by relative growth of different parts of the roots system as well as frequency of branching and angles. RSA is a key determinant for root functions and is highly plastic, being controlled by genotype to environment interactions (Yu et al., 2016; Shahzad and Amtmann, 2017; Morris et al. 2017). Optimization of RSA is thus imperative for the improvement of plant resilience, particularly to soil-borne stresses such as soil drought, flooding, nutrient deficiencies, and biotic factors (Julkowska and Testerink, 2015; Lynch, 2015; Rogers and Benfey 2015). Correlation of root morphology with DNA-sequence information allows the identification of the genetic loci that underpin root features, for example through mutant screens, quantitative trait locus (QTL) analysis or genome-wide association studies (GWAS). New sequencing technology has vastly increased the amount of available genetic information, and good phenotyping assays are now required to meet the pace of these advancements. Depending on the research question, different phenotyping

approaches need to be taken, because there is a trade-off between (a) reflecting realistic environments, (b) controlling environmental factors, (c) obtaining precise information on individual parts of the root systems, and (d) throughput.

Several platforms to obtain root images from plants grown in soil (field, pots or rhizotrons) are available, together with software to capture and model the overall size and shape of the complex root systems (Lobet et al., 2011; Bucksch et al., 2014; Kalogiros et al., 2016). These studies are complemented by analyses of roots developing on synthetic surfaces, which offer more precise control and manipulation of the root environment. Open source software such as BRAT (Slovak et al., 2014; Satbhai et al., 2017) and RootTrace (Naeem et al., 2011) have been developed to precisely track the early main root growth from scanned images of Arabidopsis seedlings growing on plates. An intermediate analysis space is occupied by software such as EZ-Rhizo (Armengaud et al., 2009), archiDART (Delory et al. 2016, 2018), RootScape (Ristova et al., 2013), or the commercial WinRhizo (Arsenault et al., 1995). They have facilitated the quantitative assessment of more advanced root systems of Arabidopsis and other dicot plants, including information on lateral root features such as position, length, density and angle. This information has generated knowledge on branching patterns, rather than just primary root growth or overall shape, and has enabled large-scale phenotyping of Arabidopsis roots to investigate natural variation and responses to multiple environmental cues (Gruber et al., 2013; Kellermeier et al., 2013, 2014; Julkowska et al., 2017).

With a good range of root image analysis software in place, the next challenge is how to process the acquired numerical data in order to extract biologically meaningful and statistically valid results. Averaging across replicates is easy for some simple RSA traits, such as main root (MR) length and lateral root (LR) number, but it is less straightforward for other traits. For example, how should we calculate the mean LR length if the number of LRs differs between replicate plants? We can either average the length of all laterals in each plant before averaging across plants, or we can average individual LRs across replicates. The latter can be done either by the order of appearance (1^{st}, 2^{nd} LR etc.) or by their position on the main root (e.g. all LRs within a particular sector of the main root). There is no one ‘correct’ solution to this problem; rather, each of the approaches is more or less suited to answer a specific question. For example, the first average provides a measure of overall growth investment into lateral roots, the second provides information on how individual LRs develop, and the last approach best reflects the root shape. It is therefore important that RSA analysis software, in addition to enabling data acquisition, also offers different options for extracting

mean root traits and their variance, which can then be used as a numerical input into genetic studies or developmental models.

Another challenge is how to visually represent averaged root systems in a manner that clearly and faithfully reflects differences between genotypes or environmental conditions. Current root image analysis software packages rarely include options to visually reconstruct single-plant or mean RSAs from the measured data. In publications, the individual averaged RSA traits are usually represented in multiple bar graphs. A picture of one 'representative' root system is often included, but considering the variability and complexity of RSA it is unlikely that one individual plant can indeed be representative in all RSA traits. The reader is left with the difficult task of deducing the mean RSA from bar graphs of all individual traits.

To address these problems we have developed a new application, Root-VIS, which enables calculation and visual reconstruction of mean RSAs from measured data. We exemplify the possibilities offered by Root-VIS using data acquired with a greatly enhanced version of the previously published EZ-Rhizo program. The combined EZ-Root-VIS pipeline provides an easy procedure to capture RSA features of many individual plants and to visualize averaged RSAs for different genotypes under various environments or at different time points. Root-VIS offers a range of choices for how to calculate means and how to visually represent the average root phenotypes. For example, it allows users to calculate means of LR-related traits on a per-plant or a per-branch basis. It provides possibilities to redraw average root architectures from the extracted data or to regenerate root shapes in the form of flag plots, as well as growth-investment or LR length profiles. We have validated the utility of the EZ-Root-VIS pipeline for studying root growth dynamics, quantitative genetics, and genotype-environment interactions.

RESULTS

Description of the EZ-Root-VIS pipeline

The software is a 'standalone' implementation, compatible with all Microsoft Windows operating systems from Windows XP (SP-3) onwards, including Vista, Windows 7, 8/8.1 and 10 (in 'Classic Desktop' mode). Separate versions are available for 32-bit and 64-bit platforms. The installation package includes Root-VIS and the latest version of the EZ-Rhizo program, which has a number of additions and improvements over the original 2009 release (Armengaud et al., 2009). For example, EZ-Rhizo now accepts input images in any of the

standard formats: Windows Bitmap (BMP) files, Graphics Interchange Format (GIF), Joint Photographic Experts Group compressed images (JPEG), Portable Network Graphics (PNG) or Tagged Image File Format (TIFF) files, and at any resolution. The software presents a typical, Windows-style graphical user interface (GUI) (Supplemental Figure 1A) which will be very familiar to users of the Microsoft® Visual Studio development environment. Extensive (and context-sensitive) on-line help is included with the software (Supplemental Figure 1B). The software also provides numerous, user-selectable options for controlling the content and style of displays, and the parameters used in the reconstruction and averaging algorithms. These are adjustable via a "Settings" property sheet (Supplemental Figure 1C).

Figure 1A summarizes the work flow of RSA analysis with the EZ-Root-VIS pipeline. Images of plants grown on agar plates in 2D are usually acquired with flatbed scanners (Figure 1B), but any image-capturing device that generates sufficient contrast and resolution is suitable. First, EZ-Rhizo is used to process the images and extract numerical data of RSA features of individual roots (Figure 1C). After image cropping, conversion into black and white and background noise filtering, roots are pixelated, skeletonized, edited and detected as described before (Armengaud et al., 2009). In the new version of EZ-Rhizo, we have included an option to re-define the main root (the original version assumed the longest root path formed the MR and this is also the default setting). The numerical results of the analysis are saved in a user-selectable database, which is now in XML format, allowing easy sharing of datasets between the acquisition and analysis modules. Root-VIS then 'reads' the database generated by EZ-Rhizo and displays the files in a database window (left panel in Supplemental Figure 1A). Prior to averaging RSA data from replicate roots, Root-VIS offers the possibility to draw a visual reconstruction of any individual root in the dataset (Figure 1D), which allows the user to verify the data that were captured by the image acquisition software.

At the heart of the Root-VIS software lies the concept of the 'collection analysis', in which data extracted from the database are grouped according to the metadata parameters entered during image analysis, including genotype, media type and plant age. Analyses can be carried out with zero, one or two of these parameters being variants. The database structure displayed in the analysis window makes it easy to remove or pool individual samples or groups of samples from the analysis (Supplemental Figure 1B). The averaged root for each group can then be displayed visually using a 'reconstruction' algorithm described in more detail in the Methods section. Two types of averaged root systems can be generated; "absolute" and

"binned" (Figure 1E-F). In the 'absolute' mode, lateral roots are averaged according to their order of appearance; in the 'binned' mode, the branched zone is divided into sectors (the number of which is equal to the mean number of LRs), and the lengths of LRs in each sector ('bin') are averaged. The program also provides an option to visualize the variation between individual replicate roots in 'alpha blends' (Figure 1G). Additional visualization options are 'flag plots' (Figure 1H), which represent the overall density and shape of the root system, and LR profiles (Figure 1I), which represent the size of LRs in different parts of the root system. Flag plots are based on LR angle and LR density as well as the lengths of branched and un-branched zones of the MR as depicted in Supplemental Figure 2. For the LR profiles, the MR length is divided into a user-defined number of sections, and for each section LR length is displayed as a rectangle of appropriate size. Each of the display modes has a number of sub-options, which the user can select in the 'Settings' windows. For example, LR profiles can be chosen to show either the sum length of all LRs (LR size, LRS) or the mean LR length (LRL) in each MR sector. The former provides a measure of total growth investment into a certain part of the root while the latter reflects the local root system width. The different displays are exemplified below using experimental data. We also generated an optional plug-in module, XL-Orate, which allows users to create formatted tables of averaged trait data, including standard errors and number of replicates using Microsoft® Excel (Figure 1J, Supplemental Dataset 1), and to rapidly generate bar charts for any data generated with EZ-Rhizo and Root-VIS. The obtained datasets can now be used in a range of downstream studies including growth models, combination with physiological data, quantitative genetics and breeding.

EZ-Root-VIS captures root growth dynamics

To validate the ability of the EZ-Root-VIS pipeline to capture root system growth, we measured RSA of *A. thaliana* Col-0 plants every two days over a period of 4 to 14 days after germination (DAG). Quantitative data for 16 root traits (see Abbreviations) were obtained using EZ-Rhizo. A 3D bar chart generated for three root traits (MRL, LRL, LRD-BZ) (Figure 2A) exemplifies the difficulty of visually representing the complexity of RSA changes in bar graphs; several additional graphs would be required to represent the overall RSA. In contrast, the visual root system reconstructions implemented in Root-VIS accommodate all the root traits and represent averaged RSA (either 'absolute' or 'binned') as a single image (Figure 2B, C). In this example, the display incorporated bends into the MR path to account for the measured difference between MR path length and MR vector length (straightness). The

program accommodates any surplus of path length over vector length across equally sized bends, which are placed at LR emergence sites in the branched zone and at equal distances along the apical zone (see Methods). However, the user should keep in mind that EZ-Rhizo does not determine the number, size and position of bends, and the displayed bending pattern could look very different from the original images. To avoid over-interpretation of the displayed bending pattern it might be safer to display either path or vector length as a straight line. Therefore, in the 'Settings' property sheet, the user can toggle between displaying bends (in the MR and/or LR), or not.

Figure 2D shows the superposition of all re-constructed individual roots in alpha blends, reflecting the variation across replicates. A similar darkness of the blends indicated that the variation of RSA between individual plants did not substantially increase with plant age. The flag plots (Figure 2E) show how the root system increases over time in depth, width and density. For this figure, flag plots were produced based on absolute values of MR and LR lengths and angles, and on the slope of the linear regression of average LR lengths at the given LR positions (see Supplemental Figure 2 and Methods). The shade of the flag fill color indicates LR density with darker shades representing higher density. Finally, LRS profiles (Figure 2F) allow the reader to quickly evaluate the growth investment into LRs in different parts of the root. In this case, the MR was divided into four equal sections (quartiles). The profiles show a sharp increase of mean LRS from 8 DAG onwards, especially in the two basal quartiles of the main root. The data underpinning Figure 2, extracted using XL-Orate (Supplemental Dataset 2), provide a convenient input into root growth models.

EZ-Root-VIS reveals genotype to environment interactions

To demonstrate the effectiveness of the pipeline for capturing genotype to environment interactions, RSA data were acquired with EZ-Rhizo from replicate plants of nine Arabidopsis accessions, growing in four nutrient media: control, low phosphate (P, 20 µM), low potassium (K, 10 µM), or combined low PK media (Figure 3, Supplemental Dataset 3; for growth media see Methods). The visual reconstructions (Figure 3) generated by Root-VIS facilitate the rapid identification of interesting responses and RSA ideotypes, while Excel generated bar graphs (Figure 4) depict means and standard errors of the individual traits. As reported before (Chevalier et al., 2003; Reymond et al., 2006; Svistoonoff et al., 2007), the Shahdara accession showed a strong inhibition of MR growth in response to P limitation. An

even stronger reduction of MR length was found for T1080 despite similar MR length on control media. In most other accessions, e.g. Aitba-2 and Cerv-1, MR growth was not sensitive to P availability, and in the Ber accession, MR growth was even stimulated by decreasing P supply (Figure 3A, Figure 4A). Instead, the size of the LR system (LRS) was reduced by low P in Ber, Aitba-2 and Cerv-1 (Figure 4B), particularly in the basal (upper) quartile of the main root (LRS (0.25), Figure 3A, Figure 4D). Unlike low P, low K decreased MR length in all accessions tested, albeit to a varying extent, and caused a decrease of LRS in most accessions (Figure 3A). Exceptions to the latter were Gie-0 and N13, which already had very small LRS in control conditions.

The effects of combined P and K limitation were striking and in many cases could not have been predicted from individual deficiency effects. In accessions experiencing MR inhibition under low P (e.g. Shahdara, T1080) combined PK limitation had an additive inhibitory effect, but in several other accessions (Gie-0, Ber, N13, Aitba-2) we recorded a complete or partial reversal of the low K-induced MR inhibition by decreasing P (Figure 4A). In Cerv-1 and Dog-4, MR inhibition by low K was maintained in low PK and dominated over MR insensitivity to low P. In contrast to the genotype-dependent response of MR to single and double deficiency, lateral root system size was in all genotypes smaller in combined PK limitation than in single deficiencies (Figure 4B). LR density in the branched zone (LRD-BZ) was in most accessions stable across treatments (Figure 4C) with the exception of, Ber, N13 and Aitba-2 which showed an increase of LRD-BZ under low K. To separate the effects of LR number and LR length on total LRS, LRL profiles and flag plots were also plotted (Supplemental Figure 3). Figure 4E shows the extracted data from these profiles as bar graphs.

The re-constructed average RSAs (Figure 3B) pinpointed additional differences. For example, MR growth was more or less vertical depending on genotype and environment. In control medium, the MR angle (MRA) differed between accessions (Figure 4D), although the direction was always the same (‘positive’, see Methods for sign definition). Under low P, MRA remained similar to control in most accessions, but markedly increased in Ber, N13 and Aitba-2, and decreased in T1080. Under low K, MRAs decreased in all accessions apart from N13. In most accessions the low-K MRA phenotype was reverted back to control or to low-P phenotypes in low PK, with a notable exception of Shahdara.

In summary, the EZ-Root-VIS pipeline enabled the analysis of complex responses of various root architectural traits to either single or combined nutrient limitations. The averaged visual

representations allow the fast identification of nutrient interactions and of accessions that show particularly interesting RSA responses. It is remarkable that the relatively small number of accessions and nutrients tested here already encompass a diverse range of combinatorial phenotypic outputs.

EZ-Root-VIS enables large scale RSA genetic studies

To validate the utility of our pipeline for large scale quantitative genetic studies, we measured RSA of 147 *A. thaliana* accessions with EZ-Rhizo, and determined means of 16 root traits with Root-VIS for downstream analyses (Supplemental Dataset 4). Five plants per accession were grown on standard medium, and it took one person 13 hours to analyze all root images obtained at one time point (12 DAG) using the EZ-Root-VIS pipeline.

A normal distribution was exhibited by ten of the analyzed root traits (Supplemental Figure 4) but several traits showed a positively skewed trait distribution, including for example LR size and number. Correlation analysis revealed a high degree of inter-dependence of the RSA traits (Figure 5A). Only root angles (MRA, LRA) were relatively independent of other RSA traits although they showed correlation with the size of MR and LRs, respectively. Surprisingly, MR length was not correlated with the LR density over the MR (LRD-MR) but was negatively correlated with LR density over the branched zone (LRD-BZ). This stresses the importance of determining LR density in the branched zone rather than relating the number of LRs to the entire main root. Interestingly, LR density was also found to be negatively correlated with the length of the basal zone (BsZL). In fact, BsZL was negatively correlated with most LR traits, suggesting that the amount of main root growth before emergence of the first LR is an important determinant of other RSA features.

Hierarchical clustering was performed to classify the accessions into groups sharing similar RSA based on 15 RSA architecture traits (LR angle was excluded from this analysis due to some negative values). As shown in Figure 5B, the accessions were assigned into eight clusters (Supplemental Dataset 4). Four clusters contained only one accession (Da(1)-12, Lp2-2, N13 and Kn-0) while the largest cluster contained 73 accessions. Average LRS profiles of the central genotype of each cluster (Figure 5C) indicated different growth investment into MR and LR. Averaged RSA reconstructions revealed differences in main root angle (MRA). For example, the Sanna-2 and Mt-0 groups exhibited more positively

skewed MRs than other groups. Thus, when applied to natural variation studies, Root-VIS quickly identifies root traits that are critical determinants of the overall RSA.

To test if the data extracted with EZ-Root-VIS can facilitate genetic mapping studies, we performed GWA mapping for 16 root traits using an accelerated mixed model (AMM) implemented in the GWAPP web application (Seren et al., 2012). In total, seven unique locus-specific single nucleotide polymorphisms (SNPs) were found to be associated with various root traits at 5% FDR (Supplemental Dataset 5). Out of these one (SNP4 6374071) was associated with TRS, LRS and LRS (0.25) (Figure 6A), three were associated with basal zone length (BsZL) and one was associated with lateral root density (LRD-MR).

47 additional SNPs were identified to be associated with root traits with an adjusted threshold of $-\log_{10}(P) > 5.0$ (Supplemental Dataset 5). One of them resembled SNP4 6374071 insofar as it showed association with LRS (0.25), LRS and TRS, suggesting a strong contribution of the lateral root size in the basal quartile to the overall root size. We named the two loci Lateral Root Size Locus (LRSL) and General Regulator Factor 1 (GRF1) (Figure 6A). LRS designates a 5 kb region which harbors four candidate genes (Supplemental Figure 5B). The GRF1 locus was named after the only gene, AT4G09000 (*GRF1)*, present in a 5 kb window around the strongest associated SNPs for this region (Supplemental Figure 5A). Interestingly, *GRF1* has been reported to be downregulated during LR emergence (Voß et al., 2015), and the expression of one of the candidates in LRSL, AT4G10270, is strongly induced around the time of LR emergence and in emerged LRs (Supplemental Figure 5C-D). We therefore investigated root phenotypes of Col-0 T-DNA insertion mutants for these two genes. Indeed, the LRS profiles showed that knockout mutants for GRF1 or AT4G10270 exhibited reductions in LRS(0.25), LRS and TRS compared to wildtype plants (Figure 6B), and the extracted data confirmed that the differences were statistically significant (Figure 6C).

In addition, we characterized the root phenotypes of T-DNA insertion lines of candidate genes underlying 18 other associations (4 significant, 14 between $-\log10(p) > 5.0$ and significant threshold) in Col-0 or Col-3 background (Supplemental Dataset 6). In total, for 14 out of the 21 associations, the mutants showed significant phenotypic differences to wildtype in several root traits, including MR angle, MR length, LRD-BZ, LR number, BsZL, and apical ZL (AZL) (Supplemental Figure 6, Supplemental Dataset 6). These results confirm that the EZ-Root-VIS pipeline is a useful tool for fast gene discovery by high-throughput RSA phenotyping.

In addition, we characterized the root phenotypes of T-DNA insertion lines of candidate genes underlying 18 other associations (4 significant, 14 between $-\log_{10}(p) > 5.0$ and significant threshold) in Col-0 or Col-3 background (Supplemental Dataset 5). In total, for 14 out of the 21 associations, the mutants showed significant phenotypic differences to wildtype in root traits for which associations were initially identified, including MR angle, MR length, LRD-BZ, LR number, BsZL, and apical ZL (AZL) (Supplemental Figure 6, Supplemental Dataset 5). Some genes, such as *ALF5* and *AXR5*, were found to contribute to more RSA traits than initially highlighted by the GWAS, suggesting a more general role in root growth and development. Data for all RSA traits in all lines are provided in Supplemental Dataset 6. These results confirm that the EZ-Root-VIS pipeline is a useful tool for fast gene discovery by high-throughput RSA phenotyping.

DISCUSSION

Root-VIS is novel for its ability to average RSA traits using several different algorithms and to visually reconstruct the averaged RSA in several manners. During the development of the software, great effort has been made to create an ergonomically efficient user interface, which is a critical factor in determining the software's ease of use. Both EZ-Rhizo and Root-VIS present a Windows-style graphical user interface (GUI) that will be easy to handle for new users. Other features include numerous keyboard accelerators and the option to skip parameter-setting dialogues using the 'shift' key, and an "Undo" command to avoid having to restart processing following inadvertent errors. Such features may, at first, seem trivial but, when considering that a typical experiment may involve processing several hundred images per day, they can make an enormous difference to the overall user experience and greatly reduce problems arising from 'software fatigue'.

We have validated our pipeline to capture fairly complex RSA of 12-d-old Arabidopsis plants in multiple contexts, including time series experiments, large scale natural variation and genotype-environment interaction studies. We provide the options to extract means based on order ('absolute') or local position of the lateral ('binned'). It was noted that depending on how much LR number varied between individual plants, the different averaging methods can lead to about 10% variation in means determined for LR-related traits. Such variation can be crucial when handling a large number of genotypes since the phenotypic spectrum across accessions is continuous with relatively small differences between the individual accessions.

We do not consider one of the averaging methods to be superior to the other; instead we provide the user with both options, allowing them to consider which approach is particularly suitable to answer their questions.

We have exemplified the utility of the EZ-Root-VIS pipeline to represent the plastic responses of various Arabidopsis accessions to environmental cues, with a particular focus on LRS profiles. Indeed, this analysis helped us to identify extreme and interesting genotypes in terms of their sensitivity to P or K limitation and combined deficiency. Under the low-P conditions applied here none of the Arabidopsis accessions showed preferential growth investment into upper (basal) lateral roots despite the widespread view that low-P adapted RSA ideotypes preferentially explore residual P in the topsoil (Lynch and Brown, 2001). This suggests that the accessions have not evolved in a P-limited environment, or that they only extend laterals if they perceive an actual P gradient. Our pipeline also revealed that interactive effect of K and P limitation modulate RSA in a genotype-specific manner that could not have been predicted from measuring RSA under single deficiency or in one accession only.

We have further validated the usefulness of the EZ-Root-VIS pipeline for facilitating GWAS on RSA. A total of 56 loci controlling various root traits could be mapped at a cut-off threshold of $-\log_{10}(P) > 5.0$. We adjusted the threshold to this level for two reasons: First, known regulators affecting root traits such as IAA1/AXR5 and ALF5 were associated with LRD-BZ and MRL with a $-\log_{10}(P) > 5.0$ and < 5% FDR significance threshold, respectively. Second, some associations which are not significant at 5% FDR yet above $-\log_{10}(P) > 5.0$ have been shown to be false negatives, because multiple testing correction methods are overly conservative (Kalladan et al., 2017; Meijón et al., 2013; Müller et al., 2016). The vast majority of the loci identified here did not contain any previously known RSA regulators. Indeed, the follow-up characterization of Col-0 KO mutants pointed to several genes with function in RSA development, including AT4G09000 (*GRF1)*, AT4G10270, AT4G10570 (*UBP9)*, AT4G01550 (*NTM2)*, AT3G29300, AT5G51560 and AT3G04260 (*PTAC3)*. We also found natural variation in genes that had previously been shown to affect root traits such as AT4G14560 (*IAA1)*, AT5G22300 (*NIT4)* and AT3G23560 (*ALF5)* (Supplemental Datasets 5 and 6). The findings provide an excellent starting point for understanding the genetics of previously unresolved traits such as LRS (0.25) and MR angle, and the role of RSA in plant adaptation to their natural habitats. Studying these traits can also provide insights into fundamental biological processes. For example, MR angle studies are expected to advance

our understanding of plagiogravitropism, cell wall integrity (van der Does et al., 2017) and voltage-sensing (Kellermeier et al., 2014) as Arabidopsis mutants impaired in cellulose biosynthesis pathway or membrane depolarization show altered MR angle.

Approaches such as GWAS become highly time and cost effective if data for multiple traits can be obtained from the same experiment. Using the EZ-Root-VIS pipeline, it is currently possible to generate data for 20 root traits (more can be added) over a mapping population comprising about 150 accessions in the course of a few days. While the throughput is lower than for some other software packages (e.g. BRAT, Slovak et al., 2014) the RSAs quantified by EZ-Root-VIS can be more complex and hence more traits can be extracted. Importantly, the visual reconstructions of averaged root systems replace the need to rely on 'representative' example pictures and enable fast integration of the measured individual RSA traits into meaningful root system shapes, which can be considered a breakthrough in the field of plant root biology. Provision of averaged root system images rather than representative images in publications is critical for interpretation and follow-up studies and it may also improve the reproducibility of results between various labs. Visual root shape reconstruction can also aid breeding efforts aimed at improving plant resilience to soil-borne stresses, facilitating the selection of desired root ideotypes from large phenotypic datasets.

EZ-Rhizo and the Root-VIS have been developed over several years, and the versions released with this paper have already been beta-tested by volunteer researchers. The software therefore represents a community effort, and we will continue to make improvements in response to suggestions and requests from the academic community.

MATERIAL AND METHODS

Software development

The EZ-Rhizo and Root-VIS applications, and their various plug-in modules (collectively packaged as The Rhizo-II Root Biometrics Suite), were developed on, and for, the Microsoft® Windows® operating systems, in the C++ language, using Microsoft® Visual Studio® 2010/2017. The graphical user interface (GUI) was implemented using objects derived from the Microsoft Foundation Class (MFC) library and interaction with the XML database is built on code from the CMarkup (V-11.5) C++ XML Parser (www.firstobject.com). The The Rhizo-II Root Biometrics Suite can be downloaded from our website (www.psrg.org.uk); it is free of charge but we ask users to register their installation.

The XL-Orate plug-in is an ‘application extension module’ (dynamic link library) which is activated via the “Plug-Ins” command in the “File” menu. It was also written in C++ and developed using the same tools and coding strategy as for the main programs. It requires installation of the Microsoft Excel software on the user’s computer and interacts with \Excel directly (without user involvement) through programmed automation.

Root-VIS was developed to be used in conjunction with EZ-Rhizo. Nevertheless, in principle, any dataset can be analysed with Root-VIS so long as it is presented in the correct format and contains all the data required for the visual reconstructions. To facilitate data input from other sources Root-VIS is already compatible with RSML (Lobet et al., 2015), and procedures for enabling Root-VIS to read those data files are currently under development.

Visual reconstructions

The Root-VIS program uses a subtle, smart algorithm to reconstruct visually representative forms, (optionally) adding ‘bends’ to roots based on the available information (the length to vector ratio, and the number, position and orientation of lateral roots). We have implemented five types of average visual reconstructions of root systems in Root-VIS, named Absolute Averages, Binned Averages, Alpha Blends, Flag Plots, and LR Profiles. The information available from the database, for a main root, comprises its path length (the total length of the root, from base to apex), its vector length (the straight-line distance between base and apex), the angle of its vector from vertical (positive angles being clockwise when looking at the root from the back of the plate) and the number of lateral roots. Lengths are expressed in centimeters and angles are in degrees. For a lateral root, the information also includes its position (the distance along its parent root from its parent’s base).

Adding bending patterns

Roots are usually not straight and therefore any visualization has to accommodate the difference between path length and vector length. However, the precise bending patterns is currently not quantified by EZ-Rhizo. We have implemented different visualization options in Root-VIS consisting either in straight lines representing path or vector length or in added bends. For roots that have no sub-root, bends can be added in a pre-decided number, equally spaced along the vector’s axis, with the displacement of each point from the axis being calculated by the application of Pythagoras’ Theorem. However, for roots with one or more sub-roots, a correlation has been demonstrated between the bending of a root and the emergence of a lateral root and that lateral roots will preferentially form at bends and follow

454 an alternating directional pattern (Laskowski et al., 2008). We therefore decided to place
455 bends along the vector, not at equal intervals, but rather at points corresponding to the
456 position of each lateral root, with the direction of the off-axis displacement being determined
457 by the sign of the branch angle. If two consecutive lateral roots branch in the same direction,
458 Root-VIS adds an extra bend point between them, being displaced in the direction opposite to
459 that of the two real sub-roots. Finally, we need to allow for a degree of bending in the apical
460 part of the root: for this, we distribute the total amount of added 'bend' between the branched
461 and apical zones according to the relative lengths of these two root segments, and allow the
462 user to specify how many (equally-spaced) bends to add in the apical zone. Clearly, the
463 described procedure does not recreate the original bending pattern but applies existing
464 evidence and user's choices to fill in missing information. While the displayed bending
465 pattern will not be faithful, the approach allowed us to correctly display both path and vector
466 length in one picture.

467 **Averaged RSA; absolute and binned modes**

468 The Root-VIS program provides two different methods for calculating the averaged RSA of a
469 given dataset, which we call "absolute averaging" and "binned averaging." For absolute
470 averages, first, the mean parameters (length, vector and angle) for the main root are
471 determined by dividing the totals for all plants by the number of samples; for the angle
472 parameter, averages are formed using the absolute values (i.e. not including the sign) and the
473 modal sign is then given to the calculated mean. Next, the median number of lateral roots is
474 calculated. Then, for each lateral root, in order of appearance, its means are calculated (in the
475 same way as for the main root, with the addition of the position parameter). If a plant in the
476 dataset has less than the median number of lateral roots, zeros are given as the four parameter
477 values for any 'missing' roots, and the divisor for the parameter totals for those lateral roots
478 is reduced by one. Since LRs are numbered from base to apex in EZ-Rhizo any 'missing'
479 lateral roots will always be at the tip of the parent root.

480 For the binned averaging algorithm, first, each main root within the dataset is split into three
481 sections: the basal zone, the branched zone and the apical zone as described (Armengaud et
482 al., 2009). The path and vector lengths are then established for each of these zones and
483 accumulated across all of the roots, and the means calculated. By adding each mean, the total
484 mean path length and mean vector length of the root are determined. Next, the mean angle
485 and median number of laterals are calculated as for absolute averages. However, to calculate
486 the mean parameters for each lateral root, we first split the branched zone into a number of

sections – or bins – equal to the mean number of lateral roots. The lateral roots for each sample in the dataset are allocated to one of these bins according to their position. The mean values for LR length, vector and angle are then calculated for each bin (as before) and for visualization they are positioned at the midpoint of the bin section. This averaging algorithm takes into account that the order of appearance does not necessarily reflect where a LR is placed; for example, the 4th lateral root in one plant could be located near the top of the main root whereas in another it could be positioned in the middle. In the visual reconstruction the representative average LR is placed at the half-way point of the respective parent root segment.

Alpha blends

The RSA reconstructions do not include an indication of the amount of variance between samples in each dataset (although standard errors are included in the numerical output). The alpha blend option allows the reconstructions of the individual roots to be overlaid in a semi-transparent fashion, thus indicating the degree of variance across the dataset. By default, when creating alpha blends, the vector angles of the main roots are normalised to the average vector angle for the samples included. Additional user-selectable options also allow for the MR path lengths and/or vector lengths to be normalised.

Flag plots

The various components of a flag plot are indicated in Supplemental Figure 2; the flagpole is divided into three sections, the lengths of which are proportional to the lengths of each of the root zones (basal, branched and apical); the angles between the upper and lower edges of the flag and the pole represent the mean insertion angles of the LRs (upper edge) and the slope of the linear regression between the mean length of the LRs and their position on the main root. Alternatively, the length of the upper edge can represent the average length of the LRs, in which case the angle between the lower edge and the flagpole will not represent any directly measured RSA data. The density of the flag's fill color represents the average lateral root density – the value of which is normalized (i.e. scaled to a value between 0 and 1) within the given set of plots.

The software provides a number of options to control how to draw flag plots, including the selections described above, selections for root path or vector data, and choice of fill color.

LR profiles

The fact that EZ-Rhizo determines the position of each LR allows simple visualization of local differences in LR growth. To construct the LR profiles, the MR is divided into a user-defined number of sectors (2-10) and the LR data within each sector is represented as a rectangle over the sector. The width of the rectangle can be chosen to represent either the total LR size (added lengths of al LRs in the sector, LRS profile) or the mean length of the LRs in the sector (LRL profile).

Plant material, growth conditions, and root image processing

Arabidopsis thaliana accessions from the RegMap panel (Horton et al., 2012), and homozygous T-DNA insertion mutant lines for candidate genes and their corresponding wildtypes Col-0 or Col-3 were obtained from the Nottingham Arabidopsis Stock Centre.

Seeds were surface sterilized in absolute ethanol for 1 min and then washed for 5 min with a solution containing 2.8% sodium hypochlorite and 0.1% Tween®-20 followed by five washes with sterile distilled water. Seeds were incubated at 4°C for 5-7 days. The sterilized and stratified seeds were sown on vertical plates with minimal media (Kellermeier et al., 2014) containing 1% agar (Formedium), 0.5% sucrose and pH 5.6 (0.2 M MES/Tris). For nutrient limitation experiments concentrations of K and P were lowered to 10 µM and 20 µM, respectively, and the osmotic potential of these media was adjusted as described before (Kellermeier et al., 2014). Plants were a grown in a growth chamber at 60 % relative humidity (RH) and 20°C, with 9 h of light (120 µE m^{-2} s^{-1}). Images of each plate were acquired using a flatbed scanner at 200 dpi as previously described (Kellermeier and Amtmann, 2013). The RSA of each plant was quantified from the images using the EZ-Rhizo as described before (Armengaud et al., 2009), facilitated by some new software functions described in the Help files of the latest version of EZ-Rhizo package released with this publication.

Statistical tests

Averaged root trait data obtained from Root-VIS using the XL-Orate plugin were used for statistical analyses unless otherwise stated. Trait frequency distribution and Shapiro-Wilk test of uniformity, correlation and agglomerative hierarchical clustering analyses were performed using XLSTAT software. Genome-wide association mapping was conducted using GWAPP web interface (https://gwas.gmi.oeaw.ac.at/) with 250K SNP data and the accelerated mixed-model (AMM) algorithm method (Seren et al., 2012). Statistically significant differences

between wild type and mutant plants was assessed using a Student's *t* test (*: $p < 0.05$) using Microsoft® Excel.

Accession numbers

Sequence data from this article can be found in the Arabidopsis Genome Initiative or GenBank/EMBL databases under the following accession numbers: AT4G09000 (*GRF1)*, AT4G10270 (in locus LRS), AT4G10570 (*UBP9)*, AT4G01550 (*NTM2)*, AT3G29300 (in locus LRDB), AT5G51560 (in locus LRK-LRN), AT3G04260 (*PTAC3)*, AT4G14560 (*IAA1)*, AT5G22300 (*NIT4)*, AT3G23560 (*ALF5)*. See also Supplemental Data Sets 5 and 6.

Supplemental Data Files

The following materials are available in the online version of this article.

Supplemental Data Set 1: Numerical data for mean RSA traits, number of replicate plants and standard error extracted from Root-Vis for the root system shown in Figure 1 E, F.

Supplemental Data Set 2: Numerical data for mean RSA traits, number of replicate plants and standard error underpinning the roots shown in Figure 2.

Supplemental Data Set 3: Means and SE of RSA traits of nine Arabidopsis accessions in four nutrient conditions (data underpinning Figures 3 and 4).

Supplemental Data Set 4: Means of RSA traits of 147 Arabidopsis accessions under control conditions and assignment of accessions into eight clusters based on variation of 15 RSA traits.

Supplemental Data Set 5: Information of SNPs associated with root trait phenotypes at $-\log_{10}(p) > 5.0$. Information on T-DNA insertion lines used for validation of candidate genes underlying various associations is also included.

Supplemental Data Set 6: Means and standard errors of RSA traits of mutants of candidate genes identified through GWAS (data underpinning Figure 6 and Supplemental Figure 6).

Supplemental Figures: Supplemental Figures 1-6 with legends, including:

Supplemental Figure 1. Screenshots of the Root-VIS software

Supplemental Figure 2. Visual explanation of the data incorporated into a Root-VIS flag plot.

Supplemental Figure 3. Average lateral root length (LRL) profiles (A) and flag plots (B) of Arabidopsis accessions in four different nutrient conditions.

Supplemental Figure 4. Frequency distribution of RS traits in Arabidopsis accessions.

Supplemental Figure 5. Genes and transcript profiles for two RSA associations.

Supplemental Figure 6. GWAS candidate gene validation

Abbreviations

MRL	Main root path length
MRV	Main root vector length
MRA	Main root angle
BsZL	Basal zone length (from hypocotyl to the first lateral root)
BZL	Branched zone length
AZL	Apical zone length
TRS	Total root system
LRS	Total lateral root path length
LRS (0.25)	Total lateral root path length in the top quartile of main root
LRL	Average lateral root path length
LRL (0.25)	Average lateral root path length in the upper quartile of main root
LRN	Number of lateral roots
LRD-MR	Lateral root density over the entire main root path (LRN/MRL)
LRD-BZ	Lateral root density in the branched zone of the main root (LRN/BZL)
LRA	Lateral root angle
OAD	Overall depth

ACKNOWLEDGEMENTS

We are grateful to Geraldine Goldie who carried out preliminary consultation and programming as part of student project at the University of Glasgow. We are also grateful to Mike Blatt for his support in the development of this software. The work was funded by the BBSRC (BB/N018508/1) and by the Gatsby Charitable Trust (Sainsbury studentship to FK).

FIGURE LEGENDS

Figure 1. Overview of EZ-Root-VIS pipeline

(A) EZ-Rhizo and Root-VIS software packages provide a convenient analysis pipeline transforming root images into a numerical and statistical data output describing root system architecture.

(B) A suitable image of Arabidopsis plants growing on a vertical agar plate can be acquired with a flatbed scanner at 200 dpi.

(C) Skeletonized roots obtained after image processing with EZ-Rhizo provide the basis for quantification of RSA features by EZ-Rhizo. The obtained data is saved in a searchable database.

(D) Root-VIS re-constructs the individual roots using the data extracted by EZ-Rhizo.

(E-J) Root-VIS generates visual reconstructions of root system architecture from a user-defined set of individual roots (replicates), including absolute (E) and binned (F) average RSA, alpha blends (G), flag plots (H) and LR profiles (I). The examples shown are based on data from the five individual Arabidopsis plants shown in B. Roots images were taken at 12 DAG.

(J) For subsequent generation of graphs, statistical analyses and modelling the numerical data obtained with Root-VIS is saved and can be displayed in Excel using the XL-Orate plug-in.

Figure 2. Visual representation of RSA development over time

(A) Change of selected RSA features over time displayed in a conventional bar graph. Plotted are plant age in days after germination (x-axis), mean lateral root density over the branched zone (LRD-BZ, y-axis), mean main root length (MRL, z-axis), and mean lateral root length (LRL, color) of *A. thaliana* Col-0 plants growing on control media. Numbers of roots analyzed at each time point are given in (B).

(B-F) Root-VIS offers several options to visualize the RSA of many replicate plants; including absolute (B) and binned (C) average RSA reconstructions, superimposition of normalized RSAs in alpha blends (D) as well as shape reconstructions in the form of flag plots (E) and LRS profiles (F). All Root-VIS reconstructions shown were based on EZ-Rhizo data obtained from *A. thaliana* Col-0 plants growing in control conditions. Plant age (in days, d) and numbers of replicate roots (n) are given in (B).

Figure 3. Environment- and genotype-dependent growth investment into main root and lateral roots

Lateral root size (LRS) profiles (A) and average RSA reconstruction (B) of Arabidopsis accessions grown in control, low K, low P, and combined low P and low K (low PK) media.

Vertical lines represent the mean main root path length. The main root path was divided into four equally-sized sections and lengths of laterals were added within each section. The width of each square represents the mean LRS of 3-6 replicate plants.

Figure 4. RSA traits of Arabidopsis accessions grown in different nutrient conditions

(A-E) Means and standard errors of selected RSA features of 12-d old Arabidopsis accessions grown in control (black bars), low K (blue bars), low P (red bars), or low PK (green bars) media. The data was generated by EZ-Rhizo and means across replicates (n = 3-6 plants) were calculated with Root-VIS for (A) main root length (MRL), (B) total lateral root size (LRS), (C) lateral root density over the branched zone (LRD-BZ), (D) main root angle (MRA). (E) Means and standard errors of lateral root length (LRL) within four sections of the main root. Data were extracted from LRL profiles generated by Root-VIS and transferred to Excel using the XL-Orate plug-in.

Figure 5. Use of the EZ-Root-VIS pipeline for large-scale natural variation studies

(A) Heatmap of pairwise correlations (Pearson correlation coefficient) of 16 RSA traits in 147 *A. thaliana* accessions. Plants were grown in control conditions. The correlations between different root features were calculated using means of 5 plants for each genotype. Stars indicate significance at $P < 0.05$.

(B) Hierarchical clustering of *A. thaliana* accessions by genotype. Calculation of similarity was based on 15 mean RSA traits calculated by Root-VIS. See Supplemental Data Set 5 for the class assignment of the individual accessions.

(C) Visual reconstructions of RSA and LRS profiles of the central accession of each cluster. Accessions names are colored according to (B).

Figure 6. Genome-wide association studies for root system architecture traits

(A) Manhattan plots for GWA mapping of three RSA traits; lateral root size over the basal quartile of the main root (LRS (0.25)), total lateral root size (LRS), and total root size (TRS). The horizontal dotted line corresponds to a 5% FDR threshold. Light blue ticks labelled 'GRF1' and 'LRSL' indicate the location of the most significant associations.

(B) LRS profiles of *A. thaliana* Col-0 wildtype and mutant lines. Plants were grown on control media in three independent experiments. The total number of replicate roots contributing to each LRS profile is given in brackets.

(C) Means and standard errors (n as shown in B) of some RSA traits in wildtype Col-0 and mutant lines. Significant differences to wildtype are indicated by asterisks ($P < 0.05$).

REFERENCES

Armengaud, P., Zambaux, K., Hills, A., Sulpice, R., Pattison, R.J., Blatt, M.R., and Amtmann, A. (2009). EZ-Rhizo: Integrated software for the fast and accurate measurement of root system architecture. Plant J. **57**: 945–956.

Arsenault, J., Pouleru, S., Messier, C., and Guay, R. (1995). WinRHlZO^{TM}, a Root-measuring system with a unique overlap correction method. HortScience **30**: 906.

Bucksch, A., Burridge, J., York, L.M., Das, A., Nord, E., Weitz, J.S., and Lynch, J.P. (2014). Image-based high-throughput field phenotyping of crop roots. Plant Physiol. **166**: 470–486.

Chevalier, F., Pata, M., Nacry, P., Doumas, P., and Rossignol, M. (2003). Effects of phosphate availability on the root system architecture: large-scale analysis of the natural variation between Arabidopsis accessions. Plant. Cell Environ. **26**: 1839–1850.

Delory, B.M., Li, M., Topp, C.N., Lobet, G. (2018) archiDART v3.0: A new data analysis pipeline allowing the topological analysis of plant root systems. F1000Res. **2018**;7.

Delory, B.M., Baudson, C., Brostaux, Y., Lobet, G., du Jardin, P., Pagès, L., et al. (2016)**.** archiDART: an R package for the automated computation of plant root architectural traits. Plant Soil **398**: 351–365.

Gruber, B.D., Giehl, R.F.H., Friedel, S., and von Wirén, N. (2013). Plasticity of the Arabidopsis root system under nutrient deficiencies. Plant Physiol. **163**: 161–79.

Horton, M.W. et al. (2012). Genome-wide patterns of genetic variation in worldwide Arabidopsis thaliana accessions from the RegMap panel. Nat. Genet. **44**: 212–216.

Julkowska, M.M. and Testerink, C.(2015). Tuning plant signaling and growth to survive salt. Trends in Plant Science **20**: 586–594.

Julkowska, M., Koevoets, I.T., Mol, S., Hoefsloot, H.C., Feron, R., Tester, M., Keurentjes, J.J.B., Korte, A., Haring, M.A., de Boer, G.-J., and Testerink, C. (2017). Genetic Components of Root Architecture Remodeling in Response to Salt Stress. Plant Cell: tpc.00680.2016.

Kalladan, R., Lasky, J.R., Chang, T.Z., Sharma, S., Juenger, T.E., and Verslues, P.E. (2017). Natural variation identifies genes affecting drought- induced abscisic acid accumulation in Arabidopsis thaliana. PNAS: 1–6.

Kalogiros, D.I., Adu, M.O., White, P.J., Broadley, M.R., Draye, X., Ptashnyk, M., Bengough, A.G., and Dupuy, L.X. (2016). Analysis of root growth from a phenotyping data set using a density-based model. J. Exp. Bot. **67**: 1045–1058.

Kellermeier, F. and Amtmann, A. (2013). Phenotyping jasmonate regulation of root growth. Methods Mol. Biol. **1011**.

Kellermeier, F., Armengaud, P., Seditas, T.J., Danku, J., Salt, D.E., and Amtmann, A. (2014). Analysis of the root system architecture of Arabidopsis provides a quantitative readout of crosstalk between nutritional signals. Plant Cell **26**: 1480–1496.

Kellermeier, F., Chardon, F., and Amtmann, A. (2013). Natural variation of Arabidopsis root architecture reveals complementing adaptive strategies to potassium starvation. Plant Physiol. **161**: 1421–1432.

Laskowski, M., Grieneisen, V.A., Hofhuis, H., Ten Hove, C.A., Hogeweg, P., Marée, A.F.M., and Scheres, B. (2008). Root system architecture from coupling cell shape to auxin transport. PLoS Biol. **6**: 2721–2735.

Lobet, G., Pagès, L., and Draye, X. (2011). A Novel image-analysis toolbox enabling quantitative analysis of root system architecture. Plant Physiol. **157**: 29–39.

Lobet G., Pound M.P., Diener J. et al. (2015) Root System Markup Language : toward an unified root architecture description language. Plant Physiol. **167**:617–627.

Lynch, J.P. (2015) Root phenes that reduce the metabolic costs of soil exploration: opportunities for 21st century agriculture. Plant, Cell Environ. **38**:1775–1784.

Lynch, J.P. and Brown, K.M. (2001). Topsoil foraging - An architectural adaptation of plants to low phosphorus availability. Plant Soil **237**: 225–237.

Meijón, M., Satbhai, S.B., Tsuchimatsu, T., and Busch, W. (2013). Genome-wide association study using cellular traits identifies a new regulator of root development in Arabidopsis. Nat. Genet. **46**: 77–81.

Morris, E.C., Griffiths, M., Golebiowska, A. , Mairhofer, S., Burr-Hersey, J. , Goh, T. , von Wangenheim, D., Atkinson, B. , Sturrock, C. J. , Lynch, J.P. , Vissenberg, K., Ritz, K. , Wells, D. M. , Mooney, S. J. , Bennett, M. J. (2017) Shaping 3D root system architecture. Curr. Biol. **27**: R919-R930

Müller, L.M., Lindner, H., Pires, N.D., Gagliardini, V., and Grossniklaus, U. (2016). A

718 subunit of the oligosaccharyltransferase complex is required for interspecific
719 gametophyte recognition in Arabidopsis. Nat. Commun. **7**: 10826.

720 **Naeem, A., French, A.P., Wells, D.M., and Pridmore, T.P.** (2011). High-throughput
721 feature counting and measurement of roots. Bioinformatics **27**: 1337–1338.

722 **Reymond, M., Svistoonoff, S., Loudet, O., Nussaume, L., and Desnos, T.** (2006).
723 Identification of QTL controlling root growth response to phosphate starvation in
724 Arabidopsis thaliana. Plant. Cell Environ. **29**: 115–125.

725 **Ristova, D., Rosas, U., Krouk, G., Ruffel, S., Birnbaum, K.D., and Corruzi, G.** (2013).
726 RootScape: landmark-based system for rapid screening of root architecture in
727 Arabidopsis. Plant Physiol. 161: 1086–1096.

728 **Rogers E.D., Benfey P.N.** *(*2015*)* Regulation of plant root system architecture: implications
729 for crop advancement. Current Opinion in Biotechnology 32: 93–98.

730 **Satbhai, S.B., Setzer, C., Freynschlag, F., Slovak, R., Kerdaffrec, E., and Busch, W.**
731 (2017). Arabidopsis root growth under iron deficiency. Nat. Commun. **8**: 1–10.

732 **Seren, U., Vilhjalmsson, B.J., Horton, M.W., Meng, D., Forai, P., Huang, Y.S., Long, Q.,**
733 **Segura, V., and Nordborg, M.** (2012). GWAPP: a web application for genome-wide
734 association mapping in Arabidopsis. Plant Cell **24**: 4793–4805.

735 **Shahzad, Z. and Amtmann, A.** (2017). Food for thought : how nutrients regulate root
736 system architecture. Curr. Opin. Plant Biol. **39**: 80–87.

737 **Slovak, R., Su, X., Shimotani, K., Shiina, T., and Busch, W.** (2014). A scalable open-
738 source pipeline for large-scale root phenotyping of Arabidopsis. **26**: 2390–2403.

739 **Svistoonoff, S., Creff, A., Reymond, M., Sigoillot-Claude, C., Ricaud, L., Blanchet, A.,**
740 **Nussaume, L., and Desnos, T.** (2007). Root tip contact with low-phosphate media
741 reprograms plant root architecture. Nat. Genet. **39**: 792–796.

742 **Van der Does, D., Boutrot, F., Engelsdorf, T., Rhodes, J., Mckenna, F., Vernhettes, S., et**
743 **al.** (2017). The Arabidopsis leucine-rich repeat receptor kinase MIK2 / LRR-KISS
744 connects cell wall integrity sensing , root growth and response to abiotic and biotic
745 stresses. PLoS Genet. 2017;13:e1006832

746 **Voß, U. et al.** (2015). The circadian clock rephases during lateral root organ initiation in
747 Arabidopsis thaliana. Nat. Commun. **6**: 7641.

748 **Yu, P. , Gutjahr, C., Li, C.J. , Hochholdinger, F.** (2016) Genetic control of lateral root
749 formation in cereals. Trends Plant Sci., 21: 951-961

750

751

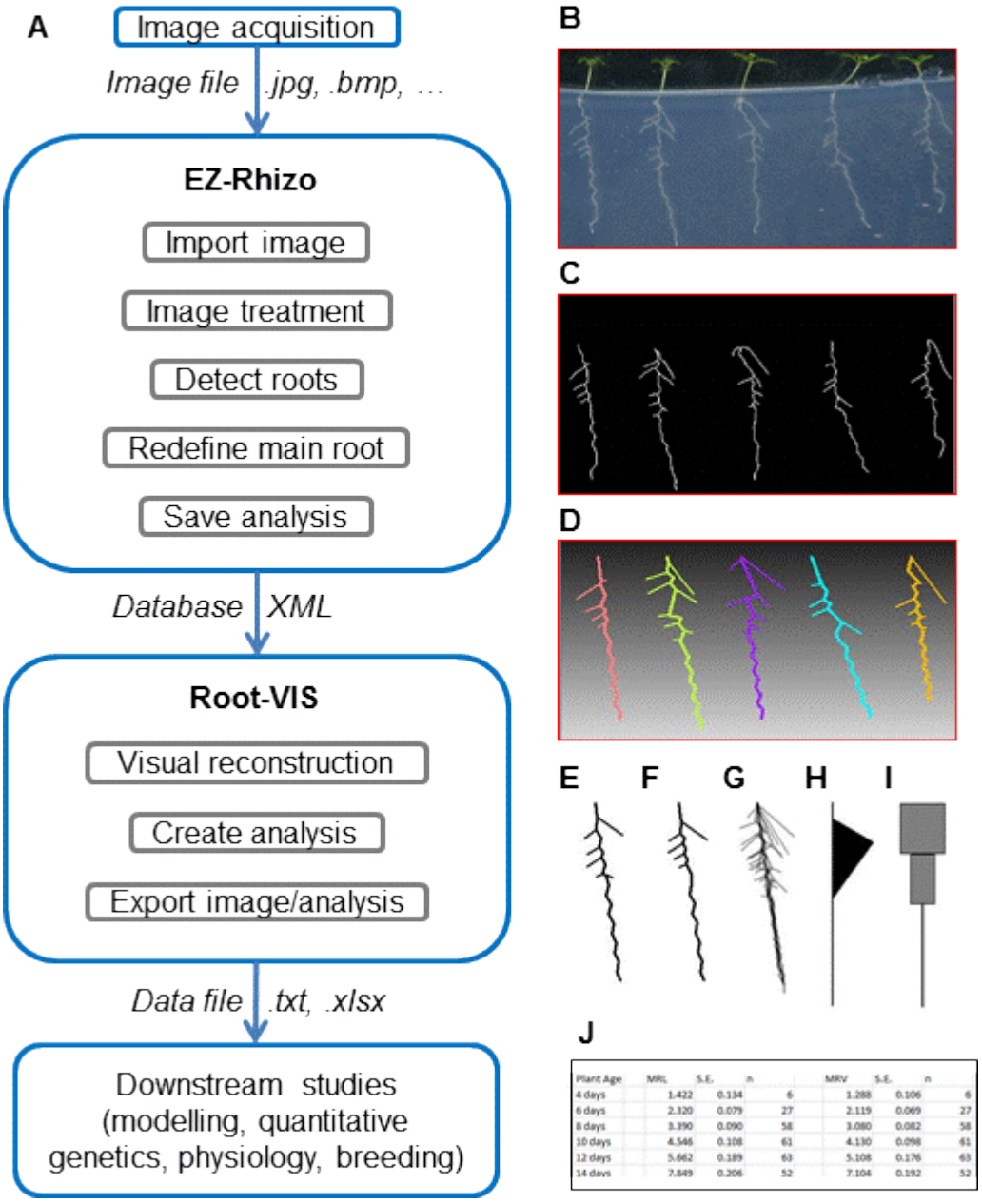

Figure 1. Overview of EZ-Root-VIS pipeline

(A) EZ-Rhizo and Root-VIS software packages provide a convenient analysis pipeline transforming root images into a numerical and statistical data output describing root system architecture.

(B) A suitable image of Arabidopsis plants growing on a vertical agar plate can be acquired with a flatbed scanner at 200 dpi.

(C) Skeletonized roots obtained after image processing with EZ-Rhizo provide the basis for quantification of RSA features by EZ-Rhizo. The obtained data is saved in a searchable database.

(D) Root-VIS re-constructs the individual roots using the data extracted by EZ-Rhizo.

(E-J) Root-VIS generates visual reconstructions of root system architecture from a user-defined set of individual roots (replicates), including absolute (E) and binned (F) average RSA, alpha blends (G), flag plots (H) and LR profiles (I). The examples shown are based on data from the five individual Arabidopsis plants shown in B. Roots images were taken at 12 DAG.

(J) For subsequent generation of graphs, statistical analyses and modelling the numerical data obtained with Root-VIS is saved and can be displayed in Excel using the XL-Orate plug-in.

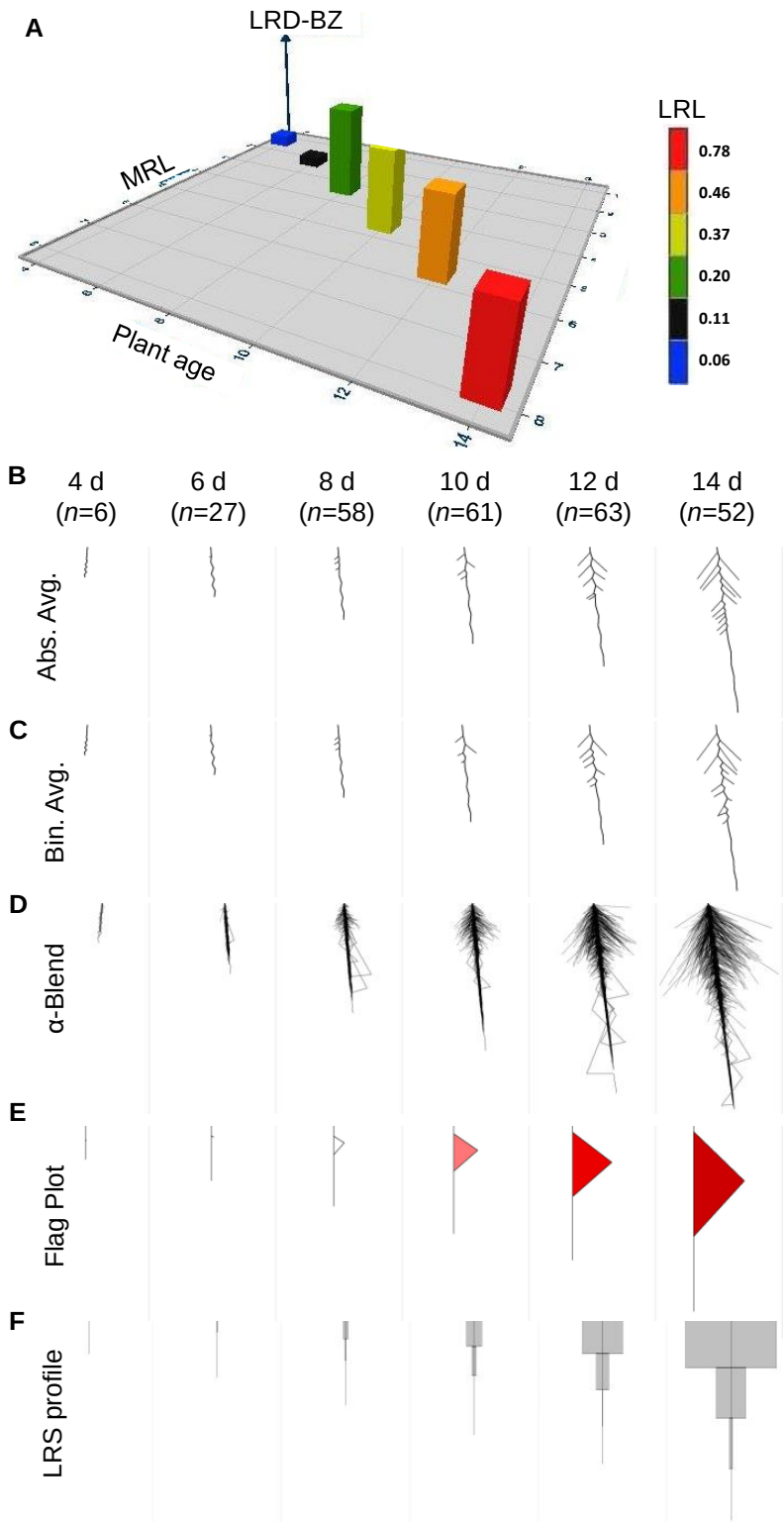

Figure 2. Visual representation of RSA development over time

(A) Change of selected RSA features over time displayed in a conventional bar graph. Plotted are plant age in days after germination (x-axis), mean lateral root density over the branched zone (LRD-BZ, y-axis), mean main root length (MRL, z-axis), and mean lateral root length (LRL, color) of *A. thaliana* Col-0 plants growing on control media. Numbers of roots analyzed at each time point are given in (B).

(B-F) Root-VIS offers several options to visualize the RSA of many replicate plants; including absolute (B) and binned (C) average RSA reconstructions, superimposition of normalized RSAs in alpha blends (D) as well as shape reconstructions in the form of flag plots (E) and LRS profiles (F). All Root-VIS reconstructions shown were based on EZ-Rhizo data obtained from *A. thaliana* Col-0 plants growing in control conditions. Plant age (in days, d) and numbers of replicate roots (n) are given in (B).

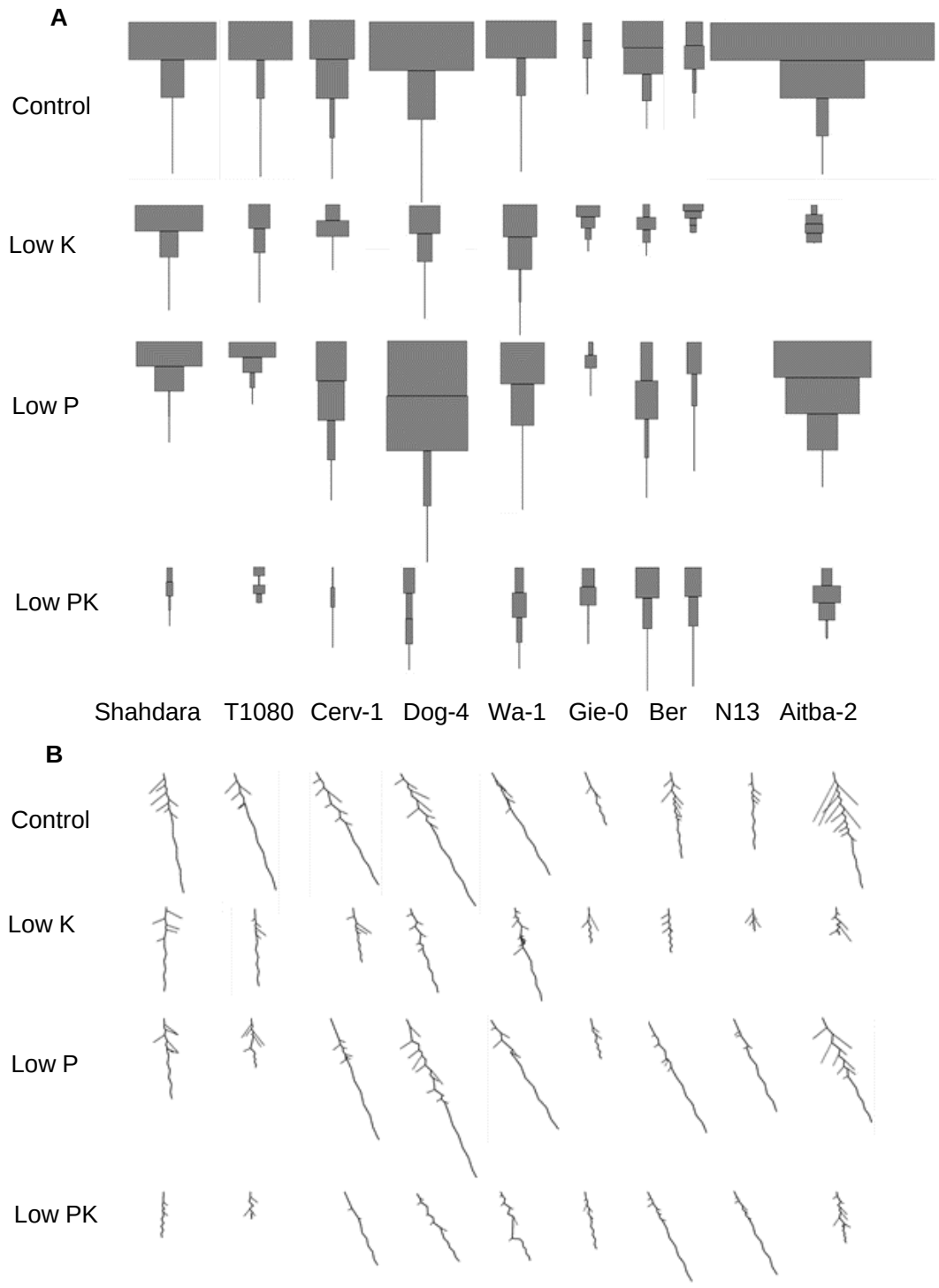

Figure 3. Environment- and genotype-dependent growth investment into main root and lateral roots

Lateral root size (LRS) profiles (A) and average RSA reconstruction (B) of Arabidopsis accessions grown in control, low K, low P, and combined low P and low K (low PK) media. Vertical lines represent the mean main root path length. The main root path was divided into four equally-sized sections and lengths of laterals were added within each section. The width of each square represents the mean LRS of 3-6 replicate plants.

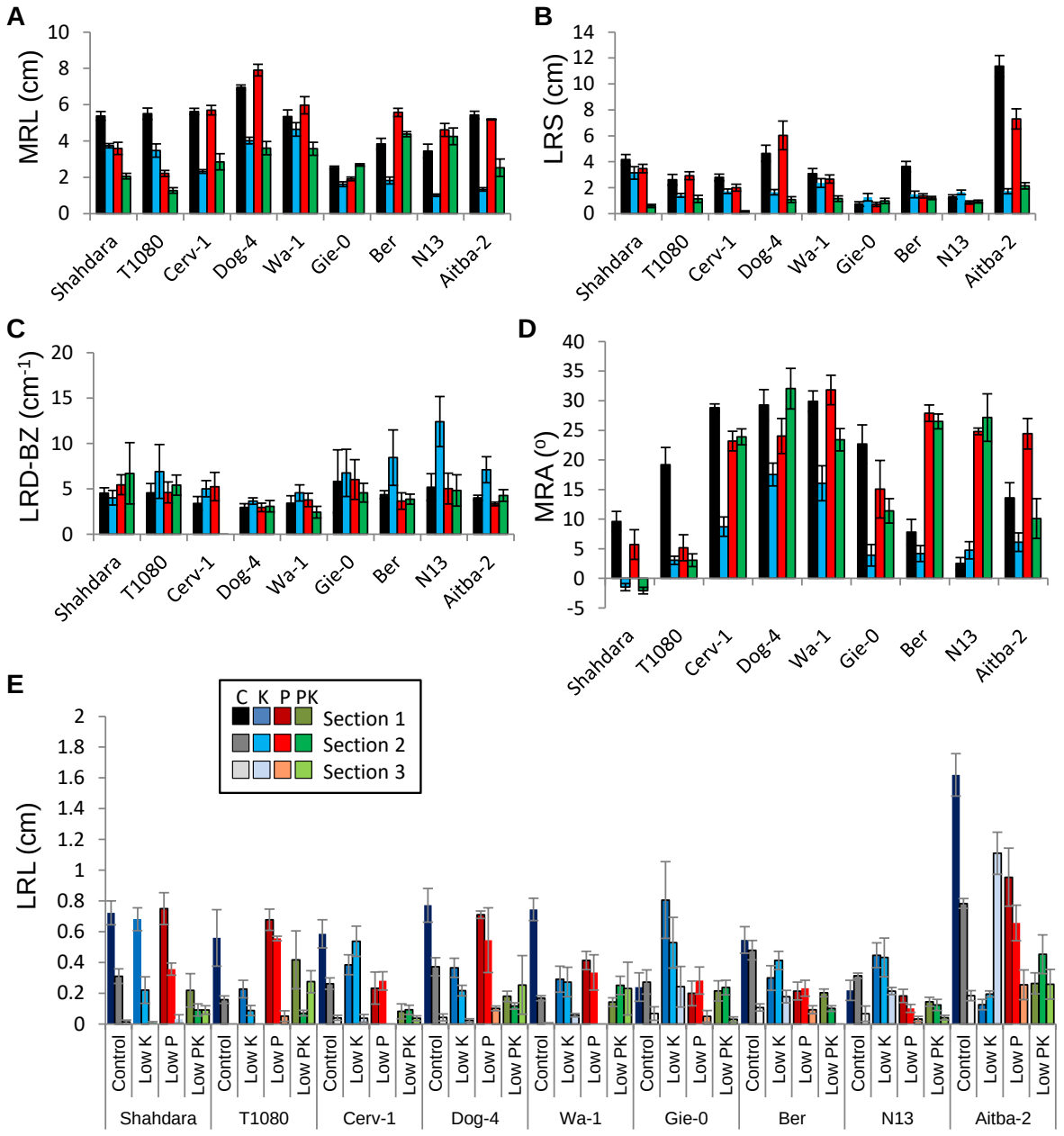

Figure 4. RSA traits of Arabidopsis accessions grown in different nutrient conditions
(A-E) Means and standard errors of selected RSA features of 12-d old Arabidopsis accessions grown in control (black bars), low K (blue bars), low P (red bars), or low PK (green bars) media. The data was generated by EZ-Rhizo and means across replicates (n = 3-6 plants) were calculated with Root-VIS for (A) main root length (MRL), (B) total lateral root size (LRS), (C) lateral root density over the branched zone (LRD-BZ), (D) main root angle (MRA). (E) Means and standard errors of lateral root length (LRL) within four sections of the main root. Data were extracted from LRL profiles generated by Root-VIS and transferred to Excel using the XL-Orate plug-in.

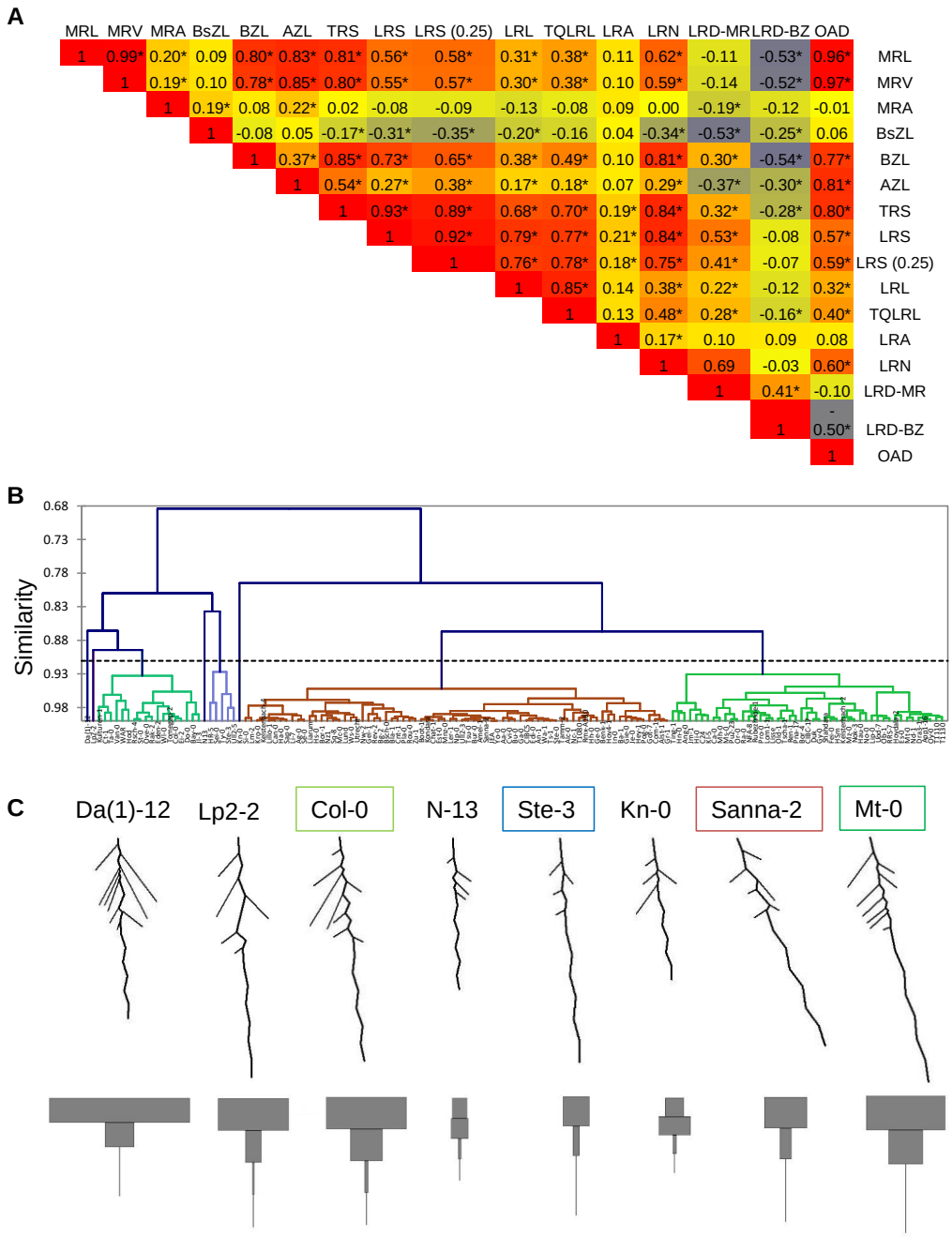

Figure 5. Use of the EZ-Root-VIS pipeline for large-scale natural variation studies
(A) Heatmap of pairwise correlations (Pearson correlation coefficient) of 16 RSA traits in 147 *A. thaliana* accessions. Plants were grown in control conditions. The correlations between different root features were calculated using means of 5 plants for each genotype. Stars indicate significance at $P < 0.05$.
(B) Hierarchical clustering of *A. thaliana* accessions by genotype. Calculation of similarity was based on 15 mean RSA traits calculated by Root-VIS. See Supplemental Data Set 5 for the class assignment of the individual accessions.
(C) Visual reconstructions of RSA and LRS profiles of the central accession of each cluster. Accessions names are colored according to (B).

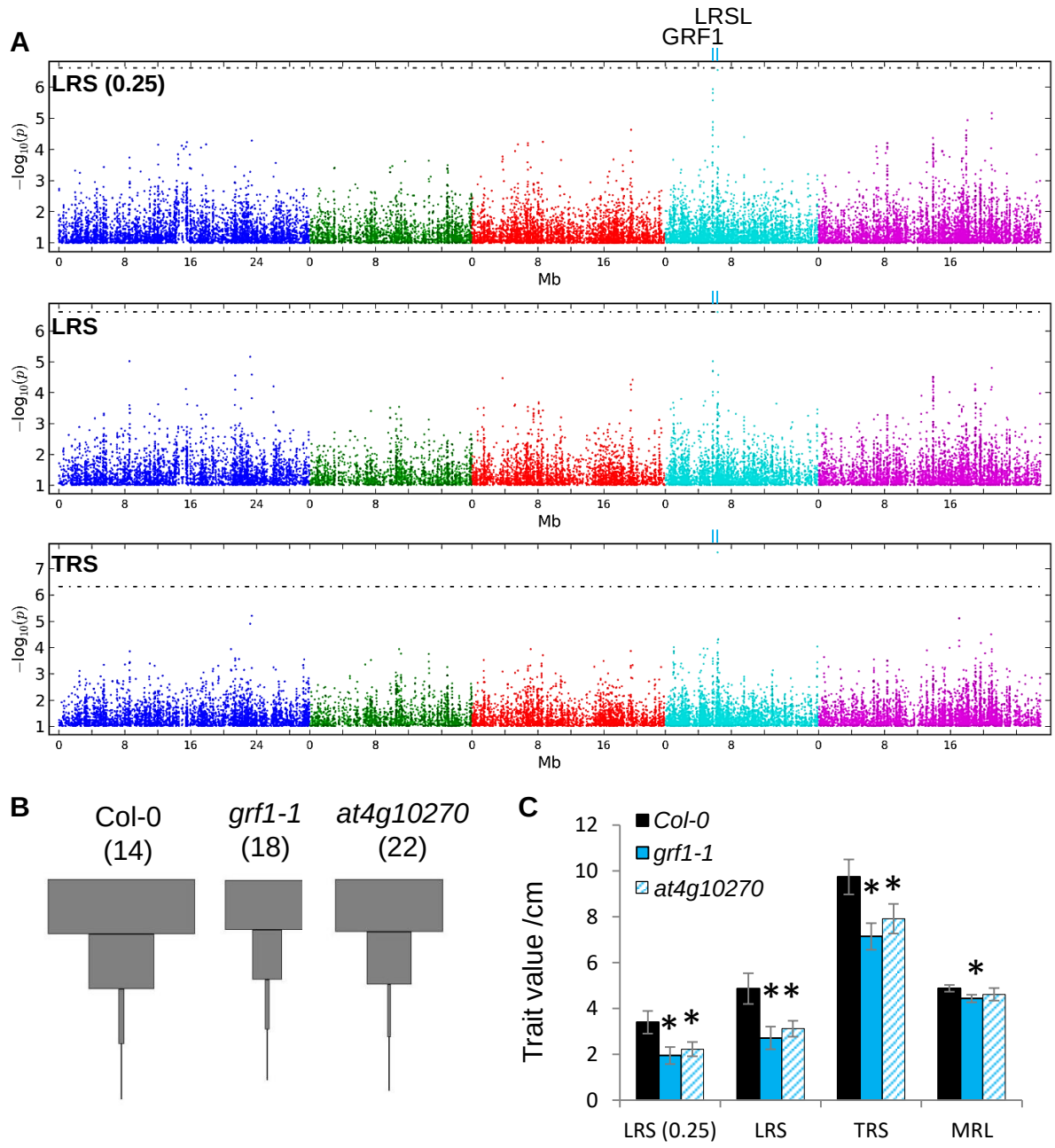

Figure 6. Genome-wide association studies for root system architecture traits

(A) Manhattan plots for GWA mapping of three RSA traits; lateral root size over the basal quartile of the main root (LRS (0.25)), total lateral root size (LRS), and total root size (TRS). The horizontal dotted line corresponds to a 5% FDR threshold. Light blue ticks labelled 'GRF1' and 'LRSL' indicate the location of the most significant associations.

(B) LRS profiles of *A. thaliana* Col-0 wildtype and mutant lines. Plants were grown on control media in three independent experiments. The total number of replicate roots contributing to each LRS profile is given in brackets.

(C) Means and standard errors (n as shown in B) of some RSA traits in wildtype Col-0 and mutant lines. Significant differences to wildtype are indicated by asterisks (P <0.05).

Parsed Citations

We are grateful to Geraldine Goldie who carried out preliminary consultation and programming as part of student project at the University of Glasgow. We are also grateful to Mike Blatt for his support in the development of this software. The work was funded by the BBSRC (BB/N018508/1) and by the Gatsby Charitable Trust (Sainsbury studentship to FK).

Armengaud, P., Zambaux, K., Hills, A., Sulpice, R., Pattison, R.J., Blatt, M.R., and Amtmann, A. (2009). EZ-Rhizo: Integrated software for the fast and accurate measurement of root system architecture. Plant J. 57: 945–956.
Pubmed: Author and Title
Google Scholar: Author Only Title Only Author and Title

Arsenault, J., Pouleru, S., Messier, C., and Guay, R. (1995). WinRHIZOTM, a Root-measuring system with a unique overlap correction method. HortScience 30: 906.
Pubmed: Author and Title
Google Scholar: Author Only Title Only Author and Title

Bucksch, A., Burridge, J., York, L.M., Das, A., Nord, E., Weitz, J.S., and Lynch, J.P. (2014). Image-based high-throughput field phenotyping of crop roots. Plant Physiol. 166: 470–486.
Pubmed: Author and Title
Google Scholar: Author Only Title Only Author and Title

Chevalier, F., Pata, M., Nacry, P., Doumas, P., and Rossignol, M. (2003). Effects of phosphate availability on the root system architecture: large-scale analysis of the natural variation between Arabidopsis accessions. Plant. Cell Environ. 26: 1839–1850.
Pubmed: Author and Title
Google Scholar: Author Only Title Only Author and Title

Delory, B.M., Li, M., Topp, C.N., Lobet, G. (2018) archiDART v3.0: A new data analysis pipeline allowing the topological analysis of plant root systems. F1000Res. 2018;7.
Pubmed: Author and Title
Google Scholar: Author Only Title Only Author and Title

Delory, B.M., Baudson, C., Brostaux, Y., Lobet, G., du Jardin, P., Pagès, L., et al. (2016). archiDART: an R package for the automated computation of plant root architectural traits. Plant Soil 398: 351–365.
Pubmed: Author and Title
Google Scholar: Author Only Title Only Author and Title

Gruber, B.D., Giehl, R.F.H., Friedel, S., and von Wirén, N. (2013). Plasticity of the Arabidopsis root system under nutrient deficiencies. Plant Physiol. 163: 161–79.
Pubmed: Author and Title
Google Scholar: Author Only Title Only Author and Title

Horton, M.W. et al. (2012). Genome-wide patterns of genetic variation in worldwide Arabidopsis thaliana accessions from the RegMap panel. Nat. Genet. 44: 212–216.
Pubmed: Author and Title
Google Scholar: Author Only Title Only Author and Title

Julkowska, M.M. and Testerink, C.(2015). Tuning plant signaling and growth to survive salt. Trends in Plant Science 20: 586–594.
Pubmed: Author and Title
Google Scholar: Author Only Title Only Author and Title

Julkowska, M., Koevoets, I.T., Mol, S., Hoefsloot, H.C., Feron, R., Tester, M., Keurentjes, J.J.B., Korte, A., Haring, M.A., de Boer, G.-J., and Testerink, C. (2017). Genetic Components of Root Architecture Remodeling in Response to Salt Stress. Plant Cell: tpc.00680.2016.
Pubmed: Author and Title
Google Scholar: Author Only Title Only Author and Title

Kalladan, R., Lasky, J.R., Chang, T.Z., Sharma, S., Juenger, T.E., and Verslues, P.E. (2017). Natural variation identifies genes affecting drought- induced abscisic acid accumulation in Arabidopsis thaliana. PNAS: 1–6.
Pubmed: Author and Title
Google Scholar: Author Only Title Only Author and Title

Kalogiros, D.I., Adu, M.O., White, P.J., Broadley, M.R., Draye, X., Ptashnyk, M., Bengough, A.G., and Dupuy, L.X. (2016). Analysis of root growth from a phenotyping data set using a density-based model. J. Exp. Bot. 67: 1045–1058.
Pubmed: Author and Title
Google Scholar: Author Only Title Only Author and Title

Kellermeier, F. and Amtmann, A. (2013). Phenotyping jasmonate regulation of root growth. Methods Mol. Biol. 1011.
Pubmed: Author and Title
Google Scholar: Author Only Title Only Author and Title

Kellermeier, F., Armengaud, P., Seditas, T.J., Danku, J., Salt, D.E., and Amtmann, A. (2014). Analysis of the root system architecture of Arabidopsis provides a quantitative readout of crosstalk between nutritional signals. Plant Cell 26: 1480–1496.
Pubmed: Author and Title
Google Scholar: Author Only Title Only Author and Title

Kellermeier, F., Chardon, F., and Amtmann, A. (2013). Natural variation of Arabidopsis root architecture reveals complementing adaptive strategies to potassium starvation. Plant Physiol. 161: 1421–1432.
Pubmed: Author and Title
Google Scholar: Author Only Title Only Author and Title

Laskowski, M., Grieneisen, V.A., Hofhuis, H., Ten Hove, C.A., Hogeweg, P., Marée, A.F.M., and Scheres, B. (2008). Root system architecture from coupling cell shape to auxin transport. PLoS Biol. 6: 2721–2735.
Pubmed: Author and Title
Google Scholar: Author Only Title Only Author and Title

Lobet, G., Pagès, L., and Draye, X. (2011). A Novel image-analysis toolbox enabling quantitative analysis of root system architecture. Plant Physiol. 157: 29–39.
Pubmed: Author and Title
Google Scholar: Author Only Title Only Author and Title

Lobet G., Pound M.P., Diener J. et al. (2015) Root System Markup Language : toward an unified root architecture description language. Plant Physiol. 167:617–627.
Pubmed: Author and Title
Google Scholar: Author Only Title Only Author and Title

Lynch, J.P. (2015) Root phenes that reduce the metabolic costs of soil exploration: opportunities for 21st century agriculture. Plant, Cell Environ. 38:1775–1784.
Pubmed: Author and Title
Google Scholar: Author Only Title Only Author and Title

Lynch, J.P. and Brown, K.M. (2001). Topsoil foraging - An architectural adaptation of plants to low phosphorus availability. Plant Soil 237: 225–237.
Pubmed: Author and Title
Google Scholar: Author Only Title Only Author and Title

Meijón, M., Satbhai, S.B., Tsuchimatsu, T., and Busch, W. (2013). Genome-wide association study using cellular traits identifies a new regulator of root development in Arabidopsis. Nat. Genet. 46: 77–81.
Pubmed: Author and Title
Google Scholar: Author Only Title Only Author and Title

Morris, E.C., Griffiths, M., Golebiowska, A. , Mairhofer, S., Burr-Hersey, J. , Goh, T. , von Wangenheim, D., Atkinson, B. , Sturrock, C. J. , Lynch, J.P. , Vissenberg, K., Ritz, K. , Wells, D. M. , Mooney, S. J. , Bennett, M. J. (2017) Shaping 3D root system architecture. Curr. Biol. 27: R919-R930
Pubmed: Author and Title
Google Scholar: Author Only Title Only Author and Title

Müller, L.M., Lindner, H., Pires, N.D., Gagliardini, V., and Grossniklaus, U. (2016). A subunit of the oligosaccharyltransferase complex is required for interspecific gametophyte recognition in Arabidopsis. Nat. Commun. 7: 10826.
Pubmed: Author and Title
Google Scholar: Author Only Title Only Author and Title

Naeem, A., French, A.P., Wells, D.M., and Pridmore, T.P. (2011). High-throughput feature counting and measurement of roots. Bioinformatics 27: 1337–1338.
Pubmed: Author and Title
Google Scholar: Author Only Title Only Author and Title

Reymond, M., Svistoonoff, S., Loudet, O., Nussaume, L., and Desnos, T. (2006). Identification of QTL controlling root growth response to phosphate starvation in Arabidopsis thaliana. Plant. Cell Environ. 29: 115–125.
Pubmed: Author and Title
Google Scholar: Author Only Title Only Author and Title

Ristova, D., Rosas, U., Krouk, G., Ruffel, S., Birnbaum, K.D., and Corruzi, G. (2013). RootScape: landmark-based system for rapid screening of root architecture in Arabidopsis. Plant Physiol. 161: 1086–1096.
Pubmed: Author and Title
Google Scholar: Author Only Title Only Author and Title

Rogers E.D., Benfey P.N. (2015) Regulation of plant root system architecture: implications for crop advancement. Current Opinion in Biotechnology 32: 93–98.
Pubmed: Author and Title
Google Scholar: Author Only Title Only Author and Title

Satbhai, S.B., Setzer, C., Freynschlag, F., Slovak, R., Kerdaffrec, E., and Busch, W. (2017). Arabidopsis root growth under iron deficiency. Nat. Commun. 8: 1–10.
Pubmed: Author and Title
Google Scholar: Author Only Title Only Author and Title

Seren, U., Vilhjalmsson, B.J., Horton, M.W., Meng, D., Forai, P., Huang, Y.S., Long, Q., Segura, V., and Nordborg, M. (2012). GWAPP: a web application for genome-wide association mapping in Arabidopsis. Plant Cell 24: 4793–4805.
Pubmed: Author and Title
Google Scholar: Author Only Title Only Author and Title

Shahzad, Z. and Amtmann, A. (2017). Food for thought : how nutrients regulate root system architecture. Curr. Opin. Plant Biol. 39: 80–87.
Pubmed: Author and Title
Google Scholar: Author Only Title Only Author and Title

Slovak, R., Su, X., Shimotani, K., Shiina, T., and Busch, W. (2014). A scalable open-source pipeline for large-scale root phenotyping of Arabidopsis. 26: 2390–2403.
Pubmed: Author and Title
Google Scholar: Author Only Title Only Author and Title

Svistoonoff, S., Creff, A., Reymond, M., Sigoillot-Claude, C., Ricaud, L., Blanchet, A., Nussaume, L., and Desnos, T. (2007). Root tip contact with low-phosphate media reprograms plant root architecture. Nat. Genet. 39: 792–796.
Pubmed: Author and Title
Google Scholar: Author Only Title Only Author and Title

Van der Does, D., Boutrot, F., Engelsdorf, T., Rhodes, J., Mckenna, F., Vernhettes, S., et al. (2017). The Arabidopsis leucine-rich repeat receptor kinase MIK2 / LRR-KISS connects cell wall integrity sensing , root growth and response to abiotic and biotic stresses. PLoS Genet. 2017;13:e1006832
Pubmed: Author and Title
Google Scholar: Author Only Title Only Author and Title

Voß, U. et al. (2015). The circadian clock rephases during lateral root organ initiation in Arabidopsis thaliana. Nat. Commun. 6: 7641.
Pubmed: Author and Title
Google Scholar: Author Only Title Only Author and Title

Yu, P. , Gutjahr, C., Li, C.J. , Hochholdinger, F. (2016) Genetic control of lateral root formation in cereals. Trends Plant Sci., 21: 951-961
Pubmed: Author and Title
Google Scholar: Author Only Title Only Author and Title